Chemical Physics 539 (2020) 110934

Contents lists available at ScienceDirect

Chemical Physics

journal homepage: www.elsevier.com/locate/chemphys

Ab-initio study of structural, electronic, elastic, phonon properties, and phase transition path of sodium selenite

Cihan Kurkcu[a,*], Selgin Al[b], Cagatay Yamcicier[c]

[a] Department of Electronics and Automation, Kirsehir Ahi Evran University, Kırşehir, Turkey
[b] Department of Environmental Protection Technologies, Izmir Democracy University, 35140 Izmir, Turkey
[c] Institute of Science, Gazi University, Ankara, Turkey

ARTICLE INFO

Keywords:
Phase transitions
Electronic properties
Elastic properties
Vibrational properties

ABSTRACT

The effects of pressure on structural, elastic, electronic, and vibrational properties of NaSe are studied using the SIESTA method. The dimensionless ratio, bulk modulus, elastic constants, Shear and Young modulus, and Poisson's ration are obtained for each phase. NaSe shows phase transitions from the $P6_3/mmc$ phase (T = 0 K, P = 0) to the Cmcm phase at 10 GPa and from this phase to the Pmmm phase at 22 GPa. High pressure results in an improvement in resistance towards volume and shape change. Elastic constants evaluation indicates that the $P6_3/mmc$ phase and the Cmcm phase of NaSe is mechanically stable. The B/G ratios of NaSe phases are also examined. It is found that NaSe has great ductility, however as pressure increases the ductility of NaSe decreases. Electronic and vibrational computation and analysis reveal that the $P6_3/mmc$ phase and the Cmcm phase of NaSe demonstrate metallic character and both phases are dynamically stable.

1. Introduction

High density, reliable energy storage batteries are as crucial as the production of clean and renewable energy with an increasing use of portable technological devices. The energy is stored in the form of chemical energy in these batteries. Those rechargeable batteries generally have a metal anode, a suitable electrolyte, and a cathode. Lithium (Li) and sodium (Na) are the most used anode metals for this matter along with sulfur (S) or more recently selenium (Se) cathodes. Se (group 16, VI) has been adopted as a promising candidate due to its low reactivity, high electronic conductivity compared to S, and similar electrochemical behavior with S [1,2]. Thus, there is growing attention for M-Se batteries. However, in the case of using Na anode and Se cathode, metastable phases of Na-Se batteries has been (poly-selenides) has been reported [3]. Also, selenium particles suffer from low reactivity and Coulombic efficiency owing to its electronically insulating properties and poly-selenides [3,4]. NaSe is one of these poly-selenides phases that is observed. Current research focuses on improving electrical conductivity and reactivity to mitigate these problems. Herein, we would like to investigate the effect of pressure on electronic, vibrational, mechanical, and ground-state properties of NaSe since the structural understanding of the material is vital to mitigate a problem logically. At this point, first-principles calculations have been well recognized and proven to provide valuable information about complex materials crystal structures and meta-stable phases. It also came to our attention that meta-stable phases of NaSe and the effect of pressure and temperature on critical properties of this material has never been investigated. This may be because Se is very recently introduced as a cathode material to these batteries [5,6] and has not been thoroughly investigated for complex problems yet. Thus, this study aims to reveal the effect of pressure on electronic, vibrational, elastic, and phase stability properties of NaSe. The results will provide new information and will be helpful for applications where Na and Se are used.

The structural properties of the phase transition mechanism in the presence of pressure are not well known due to the difficulties in monitoring the movements of the atoms during the experiments. Thanks to this study, every applied pressure value can be analyzed in detail and many properties of the material such as structural, electronic, elastic, and vibration can be determined to a large extent. In this way, we think that the obtained results will serve as a guide to the experimental and theoretical studies to be carried out next. Also, the material we are working with is one of the sodium chalcogenides (NaS, NaSe, and NaTe). There is a great deal of interest in such materials in recent years [7–9].

2. Method

The computations for structural, electronic, elastic, and vibrational

* Corresponding author.
E-mail address: ckurkcu@ahievran.edu.tr (C. Kurkcu).

https://doi.org/10.1016/j.chemphys.2020.110934
Received 18 March 2020; Received in revised form 22 June 2020; Accepted 16 July 2020
Available online 19 July 2020

properties of NaSe were conducted within Density Functional Theory (DFT) using the Siesta program [10]. GGA-PBE exchange-correlation function was adopted to conduct calculations [11]. Troullier-Martins type norm-conserving pseudopotentials for Na and Se atoms were utilized [12]. All computations were done using double-zeta (DZ) basis sets of localized atomic orbitals. The energy mesh cut-off, which corresponds to the spacing of the real space grid used to calculate the Hartree, exchange, and correlation contribution to the total energy and Hamiltonian, was set to be 350 Rydberg (Ry). NaSe was modeled using $3 \times 3 \times 2$ cells with periodic boundary conditions for 144 atoms supercells. The Brillouin zones (BZ) were sampled with the $8 \times 8 \times 4$, $8 \times 6 \times 4$, and $6 \times 4 \times 8$ Monkhorst-Pack k-point mesh for $P6_3/mmc$, Cmcm and Pmmm phases, respectively [13]. Structural optimizations were carried out by using the Parrinello-Rahman technique [14] until the residual force acting on all atoms was smaller than 0.01 eV/Å and the pressure was gradually increased by 2 GPa through this technique to the system. Initially, the system was relaxed at zero pressure, afterwards, pressure was gradually increased. The structure was equilibrated at each applied pressure through 1 fs. We have started from the beginning at each pressure step from the equilibrated coordinates of previous steps to make sure the pressure path to be continuous. To analyse each MD time, KPlot program was adopted and the RGS algorithm that gives detailed information about the space groups, atomic positions and lattice parameters of an analysed structure [15,16]. For the energy–volume calculations, we used the unit cells for the $P6_3/mmc$, Cmcm and Pmmm phases.

3. Results and discussion

3.1. Structural and elastic properties

Before investigating structural and elastic properties of NaSe under pressure, the ground state crystal structure is determined at 0 pressure (P = 0) and temperature (T = 0) as a hexagonal structure with space group $P6_3/mmc$. After structural optimization, the lattice parameters of this phase is obtained as a = 4.4818 Å, b = 4.4818 Å, and c = 10.7674 Å given in Table 1. To investigate the effect of pressure on lattice constants and cell volume, the pressure is applied gradually. Then, the dimensionless ratios of V/V_0 versus applied pressure are obtained and presented in Fig. 1. When a 10 GPa pressure is applied to the hexagonal structure of NaSe, a transition from this structure to an orthorhombic structure with the space group of Cmcm is seen. The lattice parameters that are obtained for this phase are; a = 4.5666 Å, b = 6.7919 Å and c = 10.0863 Å. As the pressure is continued to increase gradually, another phase transition at 22 GPa is seen. The crystal structure of NaSe goes phase transition from orthorhombic Cmcm to orthorhombic Pmmm at 22 GPa. The obtained lattice parameters of this phase are; a = 3.2406 Å, b = 3.6602 Å and c = 2.7073 Å. The crystal structures of these phases are depicted in Fig. 2. Fig. 1 shows that there is a sharp change in cell volume during phase transitions which indicates that the phase transition is first order. Besides, the ratio of V/V_0 decreases gradually with increasing applied pressure, and also lattice parameters of phases are becoming smaller, suggesting that high pressure causes a reduction in interatomic distance and as a result, an increase in electron interaction.

To identify the most stable phases of NaSe, the energy-volume calculation is also carried out and given in Fig. 3. As the energy-volume graph illustrates that the $P6_3/mmc$ phase with minimum energy is the most stable phase among them. In addition to this, transition pressures have been obtained from enthalpy change that is shown in Fig. 4. The transition pressures are obtained from energy-volume calculations. Then, this energy-volume data is fitted to the third-order Birch-Murnaghan equation of state [17,18] which is;

$$P = 1.5B_0\left[\left(\frac{V}{V_0}\right)^{-\frac{7}{3}} - \left(\frac{V}{V_0}\right)^{-\frac{5}{3}}\right] \times \left\{1 + 0.75(B_0' - 4)\left[\left(\frac{V}{V_0}\right)^{-\frac{2}{3}} - 1\right]\right\} \quad (1)$$

where P represents the pressure, V is the volume at the pressure, V_0, B_0 and B_0' are the volume, bulk modulus and its pressure derivate at 0 GPa, respectively. As figures demonstrate that the energy difference between phases is low.

The transition pressures of NaSe are obtained under hydrostatic pressure by gradually increasing the applied pressure to the structure in this study. However, the transition pressures that are obtained under hydrostatic pressure tend to be higher than experimental transition pressures. This is due to some of the simulation conditions that are used. In a general simulation system, there are no surface impacts and defects taken into account owing to periodic boundary conditions and ideal crystal structures. Another factor that affects transition pressures might be the time scale. Simulation time scale usually shorter than the actual experimental time scale. In a relatively short simulation time scale, the structure may not have enough time to reconstruct or relax, thereby frozen states in the simulation may form [19–21]. Therefore, it is worthwhile to compute the transition pressures from thermodynamic calculations as well. It is reported that transition pressures that are obtained from enthalpy are much closer to experimental values [22,23]. Thus, the enthalpy of NaSe as a function of pressure is calculated and given in Fig. 4. Gibbs free energy (G) is used to determine which of the phases is the most thermodynamically stable;

$$G = E_{tot} + PV - TS \quad (2)$$

where E_{tot} is the total energy, P is the pressure, V is the volume and S is the entropy. The computations are done at 0 K. Thus, the 'TS' term is neglected, thereby enthalpy is;

$$H = E_{tot} + PV \quad (3)$$

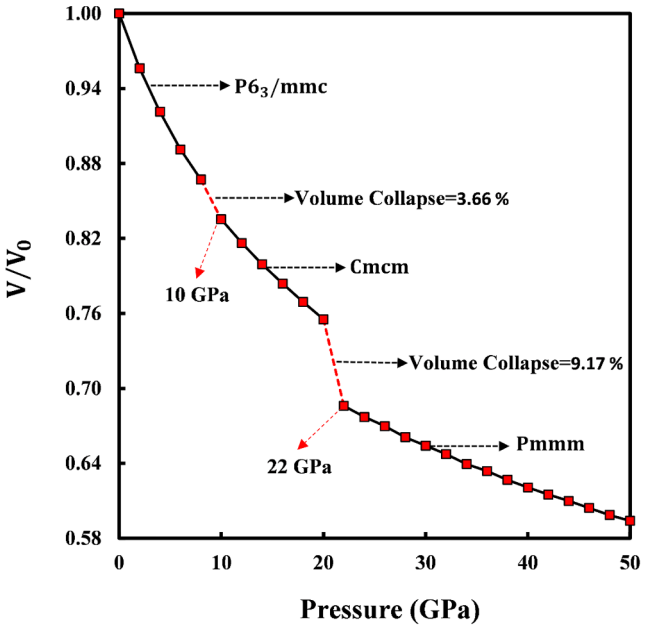

Fig. 1. The change in cell volume versus pressure.

Table 1
The values of transition pressure and lattice parameters of NaSe.

Phases	P_t (GPa)	a (Å)	b (Å)	c (Å)	c/a	References
$P6_3/mmc$	0	4.4818	4.4818	10.7674	2.4024	This Study
		3.6000	3.6000	8.4600	2.3500	[34]
		3.5300	3.5300	8.6485	2.4500	[35]
Cmcm	10	4.5666	6.7919	10.0863	–	This Study
Pmmm	22	3.2406	3.6602	2.7073	–	This Study

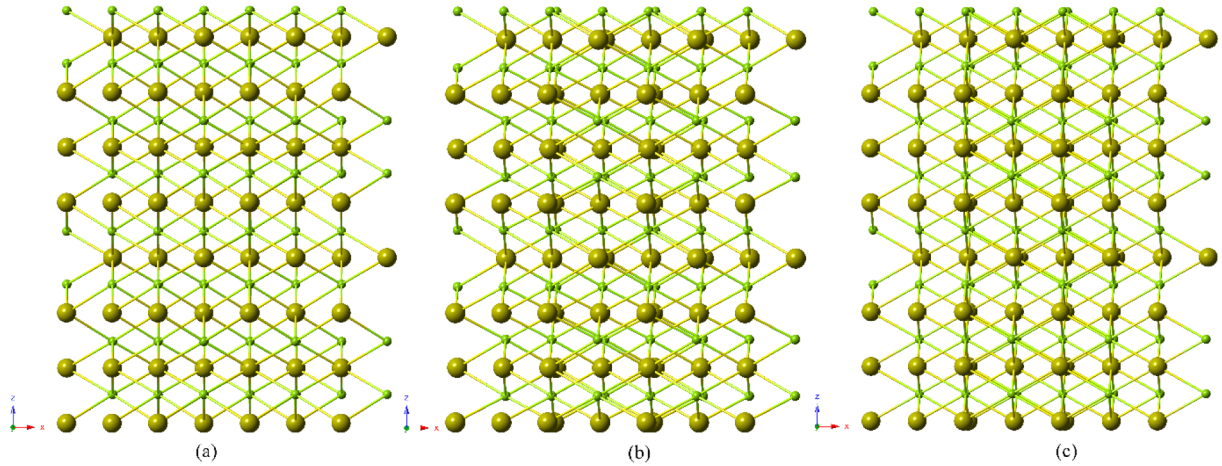

Fig. 2. Crystal structures of NaSe: (a) $P6_3/mmc$ at 0 GPa, (b) Cmcm at 10 GPa and (c) Pmmm at 22 GPa.

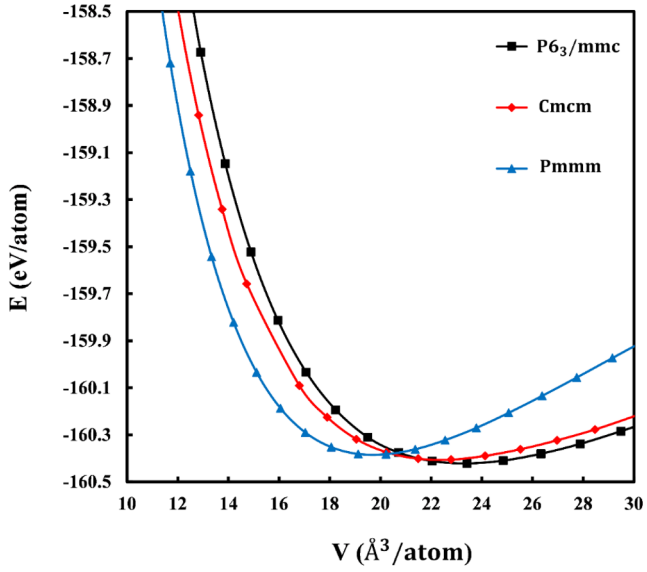

Fig. 3. The energy-volume relations of phases of NaSe.

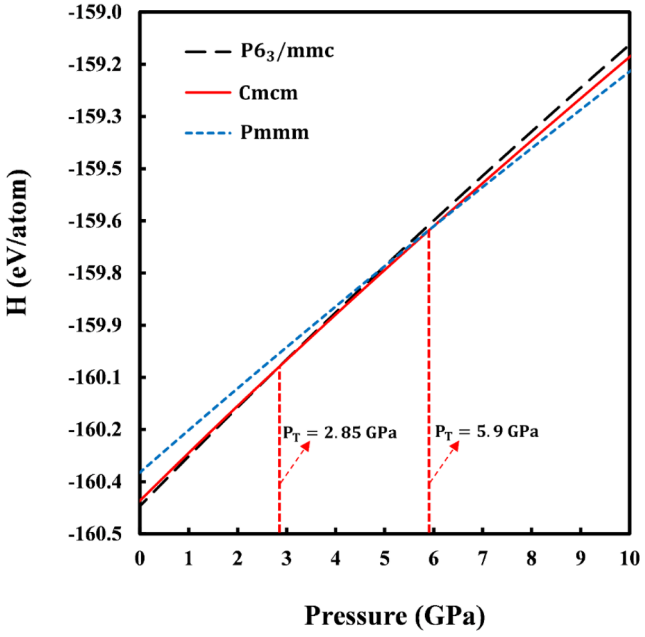

Fig. 4. Enthalpy change of phases of NaSe with pressure.

where P can be derived as $P = dE_{tot}/dV$.

The transition pressures are obtained from Fig. 4, by determining the intersection of the two enthalpies which is a sign of the phase transition containing the pressure between these two phases. The transition pressures are predicted for the phases from Fig. 4 as follows; from the $P6_3/mmc$ phase to the Cmcm phase at 2.85 GPa and from this phase to the Pmmm phase at 5.9 GPa.

The transition paths of NaSe between phases under high pressure are also studied in detail to see transformations much clearer. Each minimization step for the formation of each phase at 10 GPa and 22 GPa is analyzed with the KPlot program. In the first phase transition from $P6_3/mmc$ to Cmcm, the structure undergoes three different paths as shown in Fig. 5. On the other hand, the second phase transition follows four paths; the Cmcm to the $P2_1/m$ to the Pmma to Pmmm as displayed in Fig. 6 to reach a stable phase.

Elastic constants of a material donate the ability of the material to resist applied pressure and are very critical physical parameters in terms of determining structural stability. For a hexagonal structure, there are five independent elastic constants, namely, C_{11}, C_{12}, C_{13}, C_{33}, and C_{44}. For an orthorhombic structure, there are nine elastic constants, namely, C_{11}, C_{22}, C_{33}, C_{44}, C_{55}, C_{66}, C_{12}, C_{13}, and C_{23} [24,25]. The well-known Born criteria for the phases of NaSe is [26,27];

For a hexagonal structure,

$$C_{44} > 0, C_{11} > |C_{12}|, (C_{11} + 2C_{12})C_{33} > 2C_{13}^2 \quad (4)$$

For an orthorhombic structure,

$$C_{11} > 0, C_{22} > 0, C_{33} > 0, C_{44} > 0, C_{55} > 0, C_{66} > 0, C_{11}C_{22}C_{33} + 2C_{12}C_{13}C_{23} - C_{11}C_{23}^2 - C_{22}C_{13}^2 - C_{33}C_{12}^2 > 0, C_{11}C_{22} > C_{12}^2 \quad (5)$$

The elastic constants of NaSe phases are given in Table 2. By analyzing the data given in Table 2, it is found that the $P6_3/mmc$ hexagonal structure of NaSe and the Cmcm orthorhombic structure of NaSe are mechanically stable. On the other hand, the Pmmm structure of NaSe does not fit the well-known Born stability criteria, thus the Pmmm structure of NaSe mechanically unstable. Unfortunately, phases of NaSe under pressure and the effects of pressure on elastic constants have not been investigated previously, thus there is no data exist for comparison.

Mechanical properties of materials such as excellent resistance towards deformation, good plasticity, and strength are related to materials moduli; bulk, Shear, Young, and so on. The moduli of phases are given in Table 3. Bulk modulus defines the resistance of materials towards volume change under pressure. Therefore, it can be adopted to evaluate average bong strength because it is related to cohesive energy

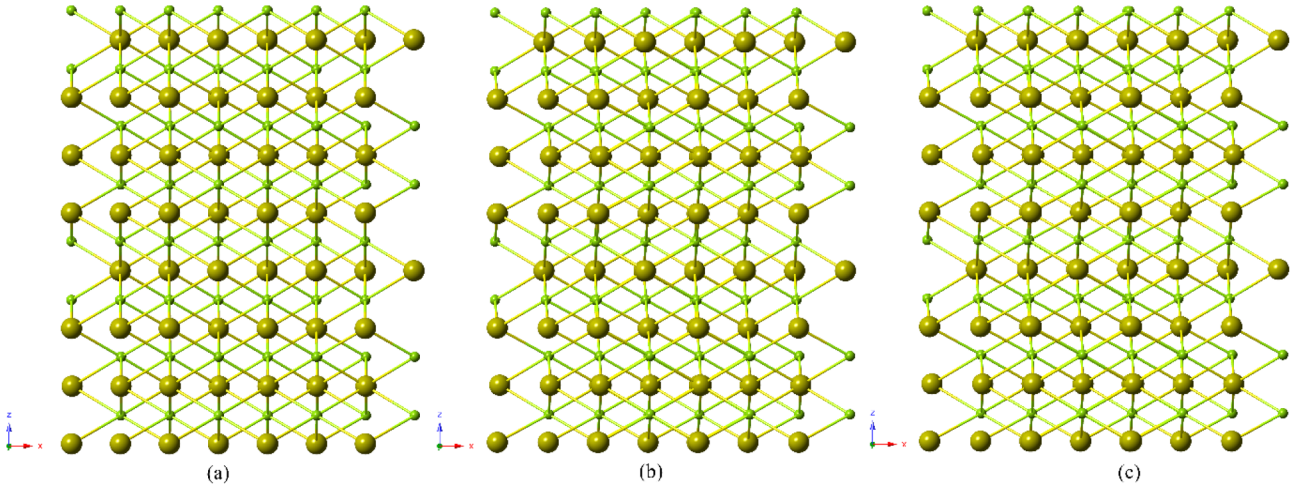

Fig. 5. Cmcm Crystal structure evolution (a) $P6_3/mmc$, (b) $P2_1/m$, and (c) Cmcm.

or binding energies of atoms within the material. A large bulk modulus has high resistance towards deformation [24,28]. Table 3 indicates that the Cmcm phase of NaSe has a greater bulk modulus than that of the $P6_3/mmc$, which means that the Cmcm phase is much mechanically stable than $P6_3/mmc$ phase.

Shear modulus of materials donates the ability to resist shape change under pressure. By examining the Shear modulus of two phases, it can be predicted that the Cmcm phase of NaSe shows greater hardness than the $P6_3/mmc$ phase due to the fact that the Cmcm phase higher Shear modulus. This prediction is also in accordance with B values.

To further study structural phase transitions and mechanical stabilities of phases, the ductile-brittle properties of the material are also considered. This property is examined by the B/G ratio. Pugh [29] stated that the B/G ratio can be considered as a key physical quantity to measure ductile-brittle properties for a polycrystalline material. The B/G ratio of 1.75 is the distinguishing point for ductility and brittleness of materials. The material is classified as ductile if the $B/G > 1.75$, it is classified as brittle if the $B/G < 1.75$. Furthermore, materials ductility increase with increasing B/G ratio, otherwise brittleness increases with decreasing B/G ratio. By looking at the data in Table 3 that NaSe has a 4.25 B/G ratio at 0 GPa in the $P6_3/mmc$ phase, however as applied pressure increases this ratio goes down to 3.30 for the Cmcm phase at 10 GPa. Since both B/G ratio is higher than 1.75, NaSe is ductile in both phases. Thus, NaSe has great ductility, however as pressure increases the ductility of NaSe decreases.

To study the plasticity of material under pressure, Poisson's ratio is also calculated. Poisson's ratio generally gives information about the interatomic bonding properties of the material. The larger the Poisson's ratio, the better material's plasticity [30,31]. This ratio is generally between -1 and 0.5. It is identified as 0.1 for covalent materials and 0.25 for ionic materials in the literature [32,33]. Poisson's ratio of NaSe is calculated as 0.36, indicating ionic bonding characteristics for this material. However, as applied pressure increases, Poisson's ratio stays the same up until a certain point. After 10 GPa applied pressure, it seems to increase.

Material's resistance towards elastic deformation denotes Young Modulus. It is defined as a ratio between tensile stress and tensile strain. As the Young modulus of material becomes larger, the stiffness of the material increases. It usually measures the resistance of the material in x-direction under applied pressure. From Table 3, it can be said that pressure increases the Young modulus of NaSe, thereby strength towards elastic deformation.

3.2. Electronic and phonon properties

To further investigate the electronic and bonding properties of NaSe, electronic band structures are obtained for $P6_3/mmc$, Cmcm, and Pmmm phases along with the high symmetry directions and presented in Fig. 7. Fermi energy level is set to 0 eV and marked with a red line in figures. As can be seen from Fig. 7a that NaSe at the $P6_3/mmc$ phase has a band gap of 0.54 eV where other phases of NaSe do not have a band gap. This means that the $P6_3/mmc$ phase shows semiconducting characteristics while other phases display metallic. Moreover, the $P6_3/mmc$ phase of NaSe is a semiconductor with direct band transition since both the valence and the conduction band are at the same point (??). As

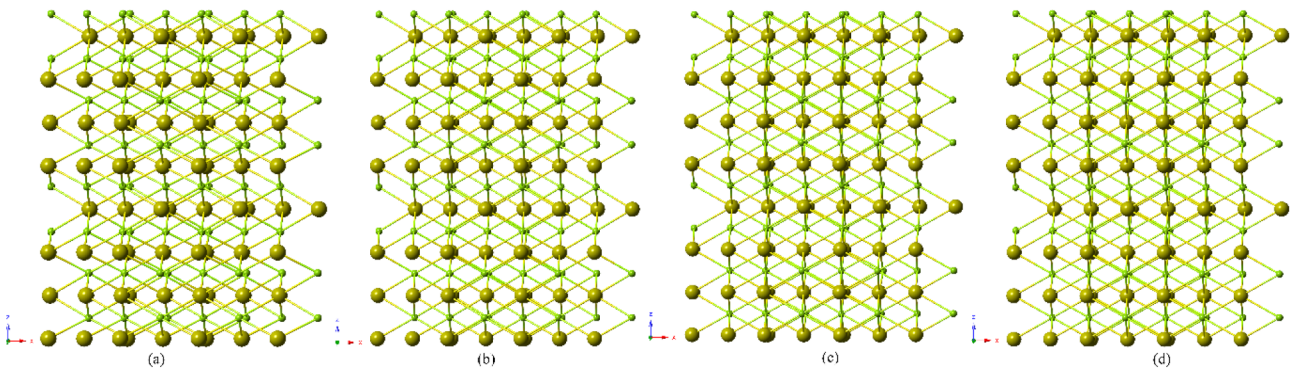

Fig. 6. Pmmm Crystal structure evolution (a) Cmcm, (b) $P2_1/m$, (c) Pmma, and (d) Pmmm.

Table 2
The obtained elastic constants (GPa) of phases of NaSe.

Phases	C_{11}	C_{22}	C_{33}	C_{44}	C_{55}	C_{66}	C_{12}	C_{13}	C_{23}
$P6_3/mmc$	48.30	–	56.47	4.06	–	14.99	40.17	16.63	–
Cmcm	107.22	49.32	110.31	9.03	23.63	40.09	67.05	38.80	40.2
Pmmm	83.28	155.63	181.03	58.59	37.23	30.00	97.40	111.96	32.90

Table 3
The Bulk modulus (B), Shear modulus G (GPa), G/B and B/G ratios, Poisson's ratios (σ) and Young's modulus E (GPa) of phases.

Phases	B	G	G /B	B/G	σ	E
$P6_3/mmc$	33.13	7.79	0.24	4.25	0.36	26.73
Cmcm	48.42	14.58	0.30	3.30	0.36	39.69
Pmmm	100.56	−83.75	−0.83	−1.20	1.07	−347.8

applied pressure is continued to increase, the valence band energy increases whereas conduction band energy decreases, which results in a decrease in band gap between valence and conduction band, even disappearance of the band gap. This leads to a reduction in the stability of crystal structure at a certain point which is in accordance with previous results.

The partial and total density of states of phases of NaSe has also been calculated. Fig. 8a, b, and c depict the density of states for the $P6_3/mmc$ phase at 0 GPa, Cmcm at 10 GPa, and Pmmm at 22 GPa, respectively. In light of DOS of NaSe, the contributions to DOS are mainly due to Se-4p states for all phases below the Fermi level. On the other hand, Na-3s and Se-4p states contribute to DOS above the Fermi level in all phases.

The phonon dispersion curves of NaSe at 0 GPa and 10 GPa are calculated and presented in Fig. 9a and b. Since the unit cell of the $P6_3/mmc$ phase of NaSe contains eight atoms and a 3 N degree of freedom, the corresponding number of vibration modes is twenty-four, as seen in Fig. 9a, of which three are acoustic modes and the remaining twenty-one are optical modes. The Cmcm phase of NaSe contains sixteen atoms in unit cell; the corresponding number of vibration modes is forty-eight, as seen in Fig. 9b, of which three are acoustic branches and the remaining forty-five are optical modes. However, as can be seen from Fig. 9a, the number of vibration modes decreases to 16 due to the binary degenerate condition between Γ – M – K – Γ – A – L high symmetry points. The number of vibration modes is 8 between L-H. In Fig. 9b, the number of vibration modes has decreased to 24 due to the binary degenerate condition between the S-R-Z-*T*-Y high symmetry points. The phonon curves of two phases ($P6_3/mmc$ phase at 0 GPa, Cmcm at 10 GPa) show no imaginary frequency, indicating that both phases of NaSe are dynamically stable. The phonon dispersion curve of the Pmmm phase of NaSe has not been computed since this phase showed mechanical instability in the analysis of elastic constants, thereby it would also display dynamical instability.

4. Conclusion

The purpose of this study is to investigate phase transitions of NaSe under high pressure and reveal the effects of pressure on structural, elastic, electronic, and vibrational properties. Calculations revealed that NaSe undergoes a phase transition and structural deformation under pressure. After a critical pressure point when applied pressure exceeds 22 GPa, the structure loses its mechanical and dynamic stability. However, high pressure seems to improve resistance towards volume and shape change since bulk and shear modulus are increasing with the applied pressure. The $P6_3/mmc$ phase and the Cmcm phase of NaSe shows ionic characteristics. Electronic band graphs of both phases indicate that NaSe depicts metallic behavior in these phases. As phonon dispersion curves of both phases show no imaginary frequency, it can be said that NaSe is dynamically stable in these phases as well. As far as the authors' knowledge this kind of study is the first study that has been carried out on the effects of high pressure on structural and mechanical properties of NaSe.

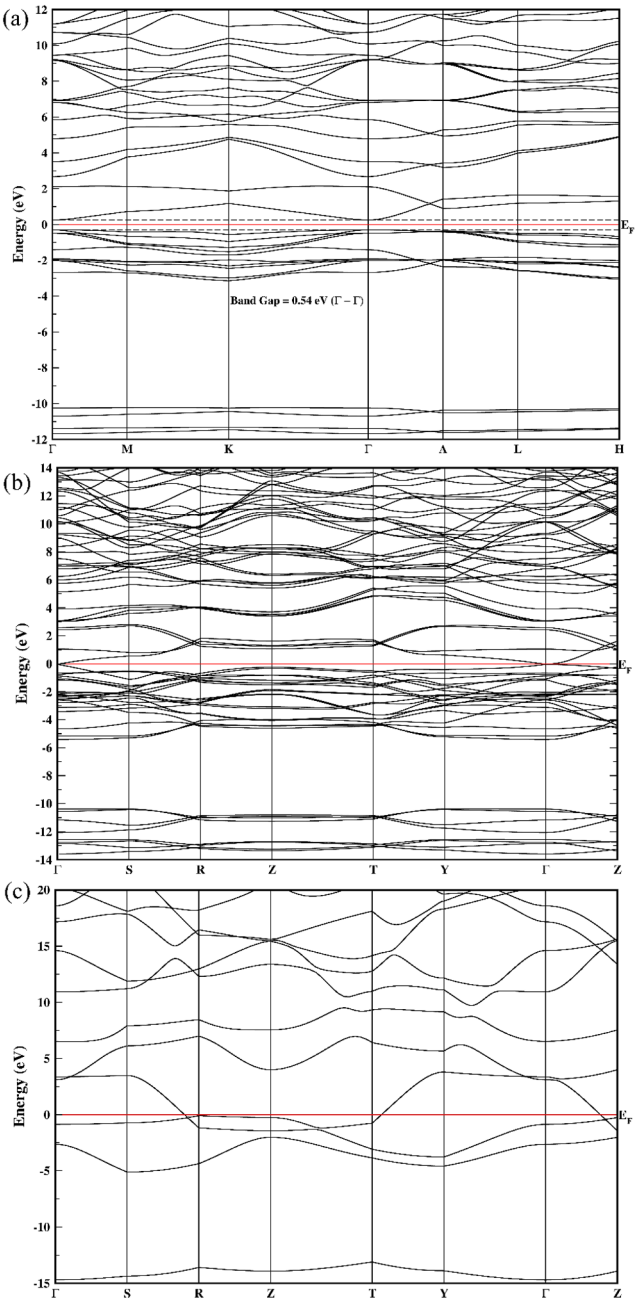

Fig. 7. The electronic band structures of NaSe at 0 GPa (a), at 10 GPa (b) and at 22 GPa (c).

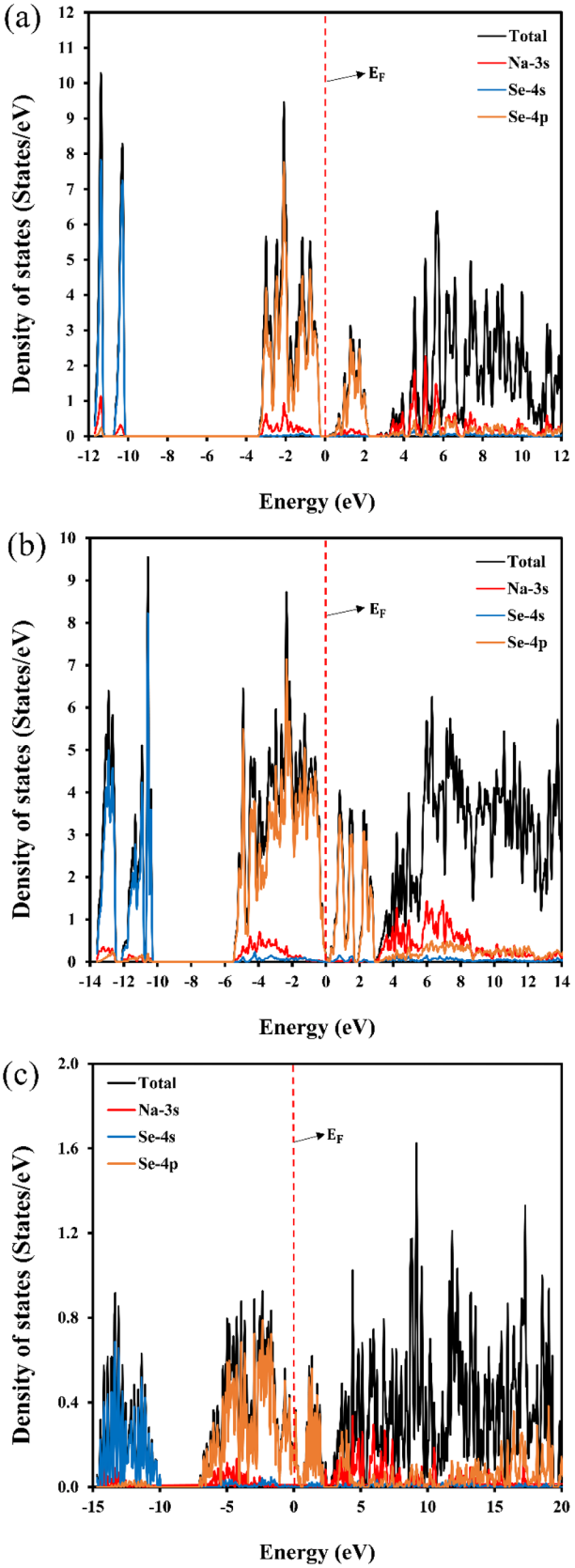

Fig. 8. The partial and total DOS of NaSe at 0 GPa (a), at 10 GPa (b) and at 22 GPa (c).

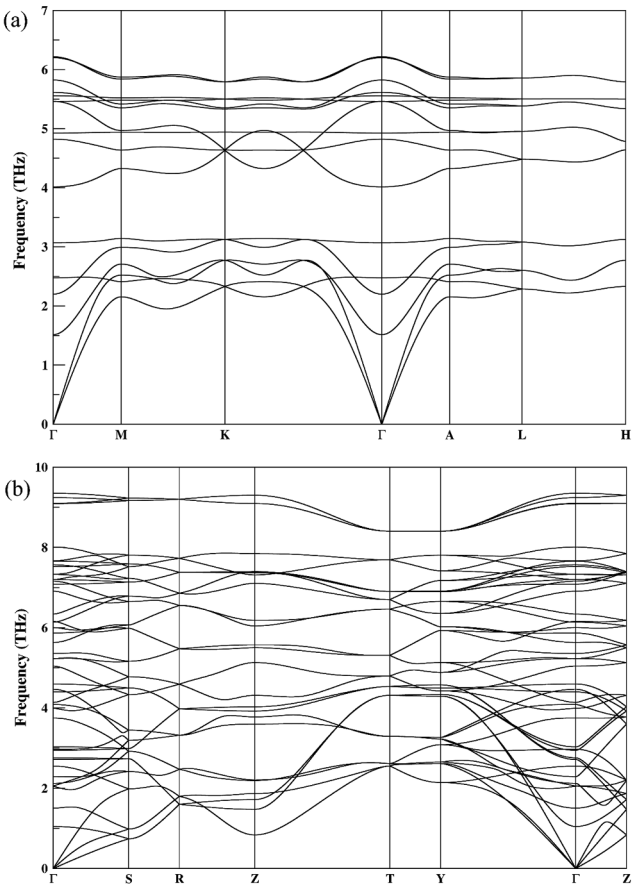

Fig. 9. The phonon dispersion curves of NaSe at 0 GPa (a) and at 10 GPa (b).

Declaration of Competing Interest

The authors declare that they have no known competing financial interests or personal relationships that could have appeared to influence the work reported in this paper.

References

[1] A. Singh, V. Kalra, J. Mater. Chem. A 7 (2019) 11613–11650.
[2] A.G. Morachevskii, Russ. J. Appl. Chem. 89 (2016) 1043–1053.
[3] H. Wang, Y. Jiang, A. Manthiram, Adv. Energy Mater. 8 (2018) 1701953.
[4] H. Wang, S. Li, Z. Chen, H.K. Liu, Z. Guo, RSC Adv. 4 (2014) 61673–61678.
[5] C. Luo, Y. Xu, Y. Zhu, Y. Liu, S. Zheng, Y. Liu, A. Langrock, C. Wang, ACS Nano 7 (2013) 8003–8010.
[6] J. Ding, H. Zhou, H. Zhang, T. Stephenson, Z. Li, D. Karpuzov, D. Mitlin, Energy Environ. Sci. 10 (2017) 153–165.
[7] T. Seddik, R. Khenata, A. Bouhemadou, N. Guechi, A. Sayede, D. Varshney, Y. Al-Douri, A.H. Reshak, S. Bin-Omran, Physica B 428 (2013) 78–88.
[8] D. Rached, M. Rabah, N. Benkhettou, R. Khenata, B. Soudini, Y. Al-Douri, H. Baltache, Comput. Mater. Sci. 37 (3) (2006) 292–299.
[9] A. Benkabou, H. Bouafia, B. Sahli, B. Abidri, M. Ameri, S. Hiadsi, D. Rached, B. Bouhafs, N. Benkhettou, Y. Al-Douri, Chin. J. Phys. 54 (1) (2016) 33–41.
[10] P. Ordejón, E. Artacho, J.M. Soler, Phys. Rev. B 53 (1996) R10441.
[11] J.P. Perdew, K. Burke, M. Ernzerhof, Phys. Rev. Lett. 77 (1996) 3865.
[12] N. Troullier, J.L. Martins, Phys. Rev. B 43 (1991) 1993–2006.
[13] H.J. Monkhorst, J.D. Pack, Phys. Rev. B 13 (1976) 5188–5192.
[14] M. Parrinello, A. Rahman, Phys. Rev. Lett. 45 (1980) 1196.
[15] R. Hundt, J.C. Schon, A. Hannemann, M. Jansen, J. Appl. Crystallogr. 32 (1999) 413–416.
[16] A. Hannemann, R. Hundt, J.C. Schon, M. Jansen, J. Appl. Crystallogr. 31 (1998) 922–928.
[17] F. Birch, Phys. Rev. 71 (1947) 809.
[18] F. Murnaghan, Proc. Natl. Acad. Sci. U.S.A. 30 (1944) 244.
[19] H. Öztürk, M. Durandurdu, PhRvB 79 (2009) 134111.
[20] C. Yamcicier, Z. Merdan, C. Kurkcu, Can. J. Phys. 96 (2017) 216–224.
[21] C. Kürkçü, Z. Merdan, Ç. Yamçıçıer, Indian J. Phys. (2019) 1–11.
[22] C. Kürkçü, Ç. Yamçıçıer, Solid State Commun. 303 (2019) 113740.
[23] S. Al, C. Kurkcu, C. Yamcicier, Int. J. Hydrogen Energy (2019).

[24] P. Li, J. Zhang, S. Ma, Y. Zhang, H. Jin, S. Mao, MoSim 45 (2019) 752–758.
[25] S. Akbudak, A. Candan, A. Kushwaha, A. Yadav, G. Uğur, Ş. Uğur, J. Alloys Compd. 809 (2019) 151773.
[26] I.O.A. Ali, D.P. Joubert, M.S.H. Suleiman, Eur. Phys. J. B 91 (2018) 263.
[27] A. Candan, S. Akbudak, Ş. Uğur, G. Uğur, J. Alloys Compd. 771 (2019) 664–673.
[28] A. Gencer, G. Surucu, S. Al, Int. J. Hydrogen Energy 44 (2019) (1938) 11930–11931.
[29] S.F. Pugh, Philos. Magazine J. Sci. 45 (1954) 823–843.
[30] L. Liu, X. Wu, R. Wang, X. Nie, Y. He, X. Zou, Crystals 7 (2017) 111.
[31] A. Candan, J. Electron. Mater. 48 (2019) 7608–7622.
[32] V.V. Bannikov, I.R. Shein, A.L. Ivanovskii, Phys. Status Solidi (RRL) – Rapid Res. Lett. 1 (2007) 89–91.
[33] S. Al, Zeitschrift für Naturforschung A, 2019, pp. 1023.
[34] F. Ahmadian, J. Supercond. Nov. Magn. 25 (2012) 1589–1596.
[35] H. Sadouki, A. Belkadi, Y. Zoaui, S. Amari, K.O. Obodo, L. Beldi, B. Bouhafs, Int. J. Comp. Mater. Sci. Eng. 7 (2018) 1850015.